

We are IntechOpen, the world's leading publisher of Open Access books Built by scientists, for scientists

6,900

Open access books available

186,000

International authors and editors

200M

Downloads

Our authors are among the

154

Countries delivered to

TOP 1%

most cited scientists

12.2%

Contributors from top 500 universities



WEB OF SCIENCE™

Selection of our books indexed in the Book Citation Index
in Web of Science™ Core Collection (BKCI)

Interested in publishing with us?
Contact book.department@intechopen.com

Numbers displayed above are based on latest data collected.
For more information visit www.intechopen.com



Distortion in RF Power Amplifiers and Adaptive Digital Base-Band Predistortion

Mazen Abi Hussein, Yide Wang and Bruno Feuvrie
Polytechnique school of the university of Nantes (IREENA)
France

1. Introduction

Future communications systems will have to integrate multiple radio technologies in order to support a large number of wireless standards (cellular technology, WMAN, WLAN and WPAN). The concept of Software-Defined Radio (SDR) in which a common hardware platform is used to cover any communication channel in a wide frequency spectrum with any modulation and bandwidth, supports this trend (Mitola, 1995; Haykin, 2005). In light of the functional flexibility and platform programmability requirements, one of the major challenges of SDR clearly resides in energy consumption. Besides the energy constraints, spectrum is becoming also a major resource bottleneck because of the steady increase in the number of wireless users and applications. The accelerated deployment of broadband personal communication and the continuously increasing demand for higher data rates will crowd the limited and precious frequency spectrum.

The power amplifier (PA) is one of the basic building blocks that imposes both spectral and power constraints while designing SDR transmitters, mainly due to its nonlinear characteristics. In fact, SDR systems should operate with third-generation (3G) air interface standards, where non constant envelope modulation formats (e.g, M-QAM, OFDM) are required as part of their functionalities. These signals are particularly vulnerable to nonlinearity and, in this case, the PA must be backed off from its normal operating point, as a simple solution to avoid nonlinear spectral distortion. Efficiency of this system is likely to be poor and size and cost may well be greater than would otherwise be required to deliver the same output power. Therefore, linearization and efficiency enhancement techniques (Kenington, 2000; Cripps, 2006) prove essential in the realization of efficient and cost-effective PAs and/or transmitters (Kenington, 2002). Such techniques, and particularly those that are digital input in nature, are a key enabling technology without which SDR cannot succeed.

This chapter makes the following two contributions. First, it provides new elements for modeling nonlinear distortion of RF PAs by reconsidering power series analysis. This analysis has been traditionally used as an intuitive introduction to understand and quantify nonlinear phenomena. However, in order to have a tractable analysis, it would be necessary to ignore higher order terms, which affects modeling accuracy. Our approach allows us to extend this analysis to an arbitrary high order in some particular cases. More interestingly, it allows to take advantage from the static power measurements and/or the parameters found in a PA's data sheet to identify the coefficients of a relatively high order RF polynomial model. Second, we experimentally evaluate one of the most promising linearization techniques for SDR transmitters, the adaptive digital baseband predistortion technique. A measurement testbed

which is designed to be fully automatic has been used. This testbed is configured so that the computer plays virtually the role of the digital predistorter in the transmission chain.

The chapter is organized as follows. Section 2 discusses nonlinear distortion. In section 3, we present advanced analytical development validated by simulations in Matlab. Section 4 describes the measurements test bench and experimentally evaluates the performance of the adaptive digital baseband predistortion technique. Section 5 concludes and discusses some perspectives.

2. Nonlinear Distortion

In order to analyze a given system, it is relevant to represent it by a mathematical model. A linear system (Fig. 1) may be described either by its impulse response $g(t)$ or by its frequency response $G(f)$, which is the Fourier transform of $g(t)$. The output signal $y(t)$ is related to the input signal $x(t)$ and the impulse response $g(t)$ by the convolution integral, $y(t) = \int_{-\infty}^{+\infty} x(\tau)g(t - \tau)d\tau$. Equivalently, the output of the system, expressed in the frequency domain is, $Y(f) = X(f)G(f)$. Thus, a linear system modifies the spectral components of its input signal according to the special form of its frequency response $G(f)$. Modifications on the amplitude spectrum of the input signal results from a simple product ($|Y(f)| = |X(f)||G(f)|$), and those on the phase spectrum from a simple addition ($\angle Y(f) = \angle X(f) + \angle G(f)$). In order to preserve the particular form of the information-bearing signal, the output signal $y(t)$ could differ from the input signal only by a constant factor a and a constant delay τ , $y(t) = ax(t - \tau)$. Every linear system whose amplitude response is not constant or whose phase response is not linear, may incur distortion to the input signal. This is what we call linear amplitude and linear phase distortion respectively.

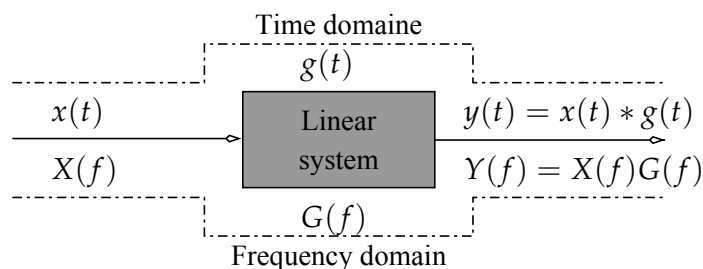


Fig. 1. Linear system

In nonlinear (NL) systems, however, a different type of distortion is encountered, which is not a simple modification of the spectral content of the input signal. Output signals are enriched with new spectral components that may be totally absent from the input signal, and they are often interpreted as an additional source of distortion (they could be exploited in some circumstances). Here, it is worthy to note that the linearity assumption on which relies the analysis of complex electronic systems is only an approximation. In reality, all circuits present some non linear effects due to design imperfections. Thus, in order to understand real phenomena encountered in electronic systems, the analysis of nonlinearity and its effects is crucial. This will be the subject of the next section.

3. Power Series Analysis

Nonlinear distortions in the transmitter are typically introduced by RF Power Amplifiers (PAs). The nonlinear behavior of this device may seriously change the properties of the trans-

mitted signals. One important and, perhaps, the simplest way for understanding and quantifying nonlinear effects of PAs, is to describe their behavior via a power series under special types of excitation signals. In this case, the power amplifier is implicitly considered as a memoryless “weakly” NL system which causes only amplitude distortion (Bosch & Gatti, 1989). In fact, when the system introduces phase distortion, it certainly possesses a certain amount of memory which cannot be taken into account by power series. Thus, we confine first our attention to nonlinear amplitude distortion. Nonlinear phase distortion will be discussed later in this chapter, through an appropriate baseband modeling of the PA.

Under the memoryless assumption, the RF output signal, denoted $y_a(t)$ (where the subscript a stands for amplitude distortion), is related to the RF input signal, $x(t)$, by the following polynomial model:

$$y_a(t) = \sum_{k=1}^{K_a} a_k x^k(t) \quad (1)$$

where the coefficients a_k are real constants that can be determined experimentally, and K_a is the polynomial (nonlinearity) order.

While traditional analysis is established in time-domain, which limits the development to lower order degrees for mathematical tractability, we propose here a novel development in the frequency domain, and give closed form expressions of the output spectrum. Such a development allows us to quantify the effect of an arbitrary high order nonlinearity on special types of test signals. Moreover, it allows to take advantage from the static power measurements and/or the parameters found in the PA’s data sheet to identify the coefficients a_k of a relatively high order RF polynomial model. The equivalent frequency-domain expression for equation (1) is

$$Y_a(f) = \sum_{k=1}^{K_a} a_k \prod_{*}^k X(f). \quad (2)$$

where $\prod_{*}^k X(f) = X(f) * X(f) * \dots * X(f)$ is the k -conv of $X(f)$, i.e. k -times the convolution product of $X(f)$.

According to the equation above, we can see that the spectrum of the output signal $Y_a(f)$ contains one term proportional to the spectrum of the input signal $X(f)$, and a set of new terms each of which is proportional to a k -conv of $X(f)$, $k = 2, 3, \dots, K_a$. Thus, one of the most obvious properties of a NL system is its generation of new frequencies absent from the input signal. If the spectrum of the input signal contains one or more frequency components, or it covers a limited bandwidth, the convolution products in (2) will multiply the number of frequency components in the first case, and spread the signal bandwidth in the second one. The formulation (2) will be analyzed and detailed in the case of special types of excitation signals: one- and two-tone signals.

We precise that, for illustration purposes, the coefficients a_k in (2) have been determined using the parameters found in the data sheet of a High power amplifier (HPA) from Mini-Circuit, the ZHL-100W-52 – (US patent 7,348,854). A 9th order polynomial model, with odd degree terms only, has been identified and used in all the simulations presented below. The model identification method will be explained later in this section.

3.1 One-Tone Signal

One simple test to describe the behavior of the PA is the one-tone test. It consists of generating a one-tone signal at the input and sweeping the power over a finite range. Analyz-

ing the spectral distortion of the output signal gives some important information which allow to quantify the degree of nonlinearity of the PA. Let us consider a one-tone input signal, $x(t) = A \cos(2\pi f_0 t)$. The Fourier transform of $x(t)$, denoted $X_{f_0}(f)$, is

$$X_{f_0}(f) = \frac{A}{2} (\delta(f - f_0) + \delta(f + f_0)). \quad (3)$$

Given the distributive property of the convolution with respect to addition, the n -conv (i.e. $\prod_*^n(\cdot)$) of X_{f_0} may be written as

$$\prod_*^n X_{f_0}(f) = \left(\frac{A}{2}\right)^n \sum_{i=0}^n \binom{n}{i} \delta(f + (n-i)f_0 - if_0). \quad (4)$$

Hence, using Eq. (4), and substituting (3) in (2), the output spectrum of the PA may be written in the form

$$Y_a(f) = \sum_{k=1}^{K_a} a_k \left(\frac{A}{2}\right)^k \sum_{i=0}^k \binom{k}{i} \delta(f + (k-2i)f_0). \quad (5)$$

We can notice the generation of a remarkable number of new components at frequencies $(k - 2i)f_0$ in Eq. 5. Each successive term generates more new frequencies than the previous one. Besides, odd (even) degree terms generate only odd- (even-) order frequency components since the parity of $k - 2i$ is equal to the parity of k . For instance, the term corresponding to $k = 3$ generates 4 frequencies at $(\pm 3f_0, \pm f_0)$, while the term corresponding to $k = 2$ generates 3 frequencies at $(\pm 2f_0, 0)$. Such new frequency components, which appear at a multiple of the original frequency f_0 , are called the *harmonics*.

3.1.1 AM/AM Characteristic

In one-tone tests, the amplitude nonlinearity which is the nonlinear relationship between the input power and the output power, could be quantified by a characteristic curve, called the *AM-AM* (Amplitude Modulation) characteristic. It is also called the *AM-AM conversion*, since it is the conversion introduced by the PA between the amplitude modulation present on the input signal, and the modified amplitude modulation present on the output signal.

In practice, this curve is obtained by measuring the output power at the fundamental frequency f_0 for different values of the average input power. Theoretically, the average power of the signal is proportional to the sum of the squares of its spectral components (Parseval's identity). Thus, given the symmetry of the spectrum around the origin $f = 0$, the average power of the one-tone signal, measured in dBm, is equal to

$$P_{avg}^{in} = 10 \log_{10} \frac{2 |X_{f_0}(+f_0)|^2}{R 10^{-3}} \quad (6)$$

where R is the resistance for terminal circuits and measurement instruments interface. It is of common use in telecommunications to choose a reference power of $1mW$ (the factor 10^{-3} in (6))¹. For the output signal, every odd-order term in Eq. (5) generates one spectral component

¹dBm is an abbreviation for the power ratio in decibel (dB) of the measured power referenced to one milliwatt (mW).

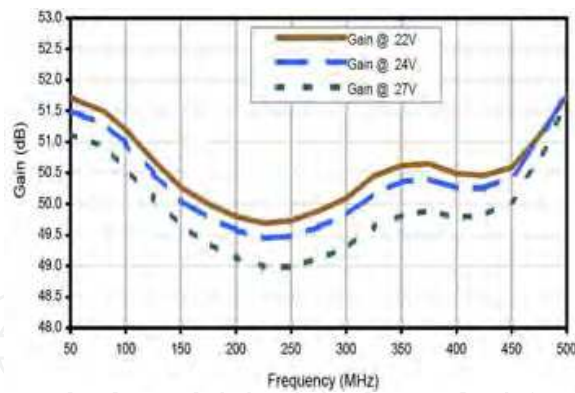


Fig. 2. Gain flatness of the ZHL-100W-52 in its operation bandwidth (data sheet, US patent 7,348,854)

at f_0 . Once again, given the symmetry around the origin $f = 0$, the power $P_{f_0}^{out}$ of the output signal at the frequency f_0 , is given by

$$P_{f_0}^{out} = 10 \log_{10} \frac{2 |Y_a(+f_0)|^2}{R10^{-3}} \quad (7)$$

where $Y_a(+f_0)$ is the amplitude of the sum of all the components at $+f_0$ in Eq. (5)

$$Y_a(+f_0) = \sum_{k=1}^K a_{2k-1} \left(\frac{A}{2}\right)^{2k-1} \binom{2k-1}{k}. \quad (8)$$

Substituting $Y_a(+f_0)$ in Eq. (7) by its value in Eq. (8), the former can be expressed in function of the average input power or the input power $P_{f_0}^{in}$ at f_0

$$P_{f_0}^{out} = P_{f_0}^{in} + G + Gc_{f_0} \quad (9)$$

where

$$G = 10 \log_{10}(a_1^2), \quad (10)$$

$$Gc_{f_0} = 10 \log_{10}(1 + S)^2, \quad (11)$$

and $S = \sum_{k=2}^K \frac{a_{2k-1}}{a_1} C_{2k-1}^k (A/2)^{2(k-1)}$. For low input power values, the Gc_{f_0} factor (11) is negligible, and the output power $P_{f_0}^{out}$ at f_0 is a linear function of the input power. In this range of power, the PA is considered to be linear. The factor G is the gain of the amplifier expressed in dB. This gain, which does not depend on the input power, varies often in function of frequency in the operating bandwidth of the PA. For instance, the typical gain of the ZHL-100W-52 is equal to 50dB (± 1.2 , typical variation) and figure 2, extracted from its data sheet, shows the gain variation in its operating bandwidth (50 – 500 MHz).

For higher input power levels, the summation S in (11) takes negative values between -1 and 0 , $-1 < S < 0$. Consequently, the factor Gc_{f_0} takes negative values incurring a gain decrease w.r.t the gain G in the linear region. Hence, the PA operates in a nonlinear mode and the notation Gc_{f_0} is chosen to indicate the amount of gain compression in the nonlinear region. The amplifier reaches finally a region of saturation, where the output power does not increase anymore with the input power.

The AM-AM characteristic of the ZHL-100W-52, modeled by the 9th-order polynomial model, is presented in figure 3. As we can see the polynomial model is unable to model the saturation region. This is one of the limitations of polynomial models which are restricted to describe the behavior of weakly NL systems. Note that the fundamental frequency has been chosen in the operating bandwidth of the PA, $f_0 = 250$ MHz. But since the polynomial model does not take into account memory effects, the choice of the fundamental frequency does not change the model behavior. In order to study NL systems with memory effects, more complicated models are required, such as the Volterra series and neural networks (Schetzen, 2006; Morgan et al., 2006; Ibnkahla, 2000; Liu et al., 2004; Wood et al., 2004; Isaksson et al., 2005).

3.1.2 Compression and Interception Points

For an ideal PA, $G_{c_{f_0}}$ in (9) is equal to zero (Fig. 3) on the whole operating power range. In order to quantify the gain compression phenomenon, the deviation of the AM/AM characteristic of the real PA from the ideal one is determined for different values of the input power (or output power) in the nonlinear operating region. The *compression points* at 1 and 3 dB are often determined and indicated in the data sheet of PAs. For instance, 1 and 3 dB compression points of our case study PA, the ZHL-100W-52, are specified in its data sheet by typical output power values of 47 and 48 respectively, as shown in Fig. 3.

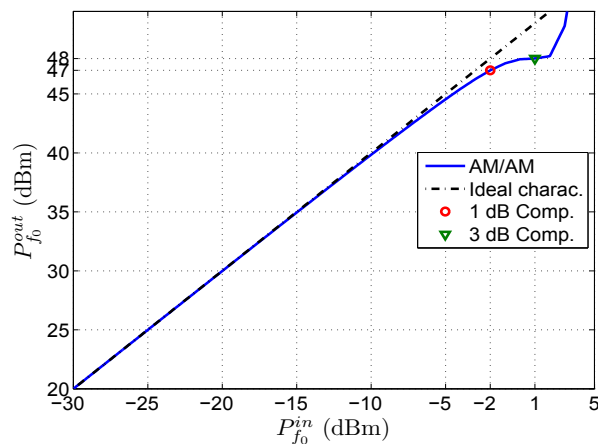


Fig. 3. AM/AM characteristic - ZHL-100W-52 modeled by a 9th degree polynomial model, with odd-order terms only

Now, let us consider the output power at the harmonic frequencies, nf_0 ($n > 1$). As mentioned before, even degree terms in (5) generate the even order harmonics, while odd order terms generate the odd order harmonics. Similarly to the development done in subsection 3.1.1, we can determine the amplitude of the the sum of all spectral components generated by all the terms of the power series at any harmonic frequency nf_0 . The value of $Y_a(f)$ (5) for positive even order harmonics $+2mf_0$, $m = 1, 2, \dots$, can be written as

$$Y_a(+2mf_0) = \sum_{k=m}^K a_{2k} \left(\frac{A}{2}\right)^{2k} \binom{2k}{k-m} \quad (12)$$

and for odd order harmonics, $Y_a(+ (2m - 1)f_0)$ can be written as

$$Y_a(+ (2m - 1)f_0) = \sum_{k=m}^K a_{2k-1} \left(\frac{A}{2}\right)^{2k-1} \binom{2k-1}{k-m}. \quad (13)$$

Then, to illustrate, the output power at any odd-order harmonic frequency $(2m - 1)f_0$ ($m = 1, 2, \dots$) can be written in a form similar to (9)

$$P_{(2m-1)f_0}^{out} = (2m - 1)P_{f_0}^{in} + G_{h_{2m-1}} + G_{Ch_{2m-1}} \quad (14)$$

where

$$G_{h_{2m-1}} = 10 \log_{10}(a_{2m-1}^2) - 32(m - 1) \quad (15)$$

and

$$G_{Ch_{2m-1}} = 10 \log_{10}(1 + S)^2. \quad (16)$$

and $S = \sum_{k=m+1}^K \frac{a_{2k-1}}{a_{2m-1}} C_{2k-1}^{k-m} (A/2)^{2(k-m)}$. Note that, in the particular case where $m = 1$, Eq. (14) is equivalent to Eq. (9). And as for Eq. (9), the factor $G_{Ch_{2m-1}}$ is negligible for low input power levels. In this region, the output power $P_{(2m-1)f_0}^{out}$ is a linear function of the input power $P_{f_0}^{in}$. Furthermore, according to (14), we observe that the output power $P_{(2m-1)f_0}^{out}$ increases $2m - 1$ times more rapidly than the output power $P_{f_0}^{out}$ at the fundamental frequency in function of the input power $P_{f_0}^{in}$. At first glance, one could expect a point for which the fundamental component and the $(2m - 1)^{th}$ harmonic have the same output power, for a given input level. However, the gain compression phenomenon on the fundamental component (9) as well as on the harmonic $(2m - 1)f_0$ (14), occurs before reaching this point. This point is called the $(2m - 1)^{th}$ *interception point* (Kenington, 2000), and is determined either at the input and, in this case, we will denote it by IP_{2m-1}^{in} , or at the output and it will be denoted IP_{2m-1}^{out} . In practice, this level can never be reached, because of the gain compression of the PA. Note that an equation equivalent to (14) can be determined for even order harmonics by repeating a similar development starting from Eq. (12). In almost all PA data sheets, only third order interception point is given. We will see below that another, more commonly used definition for the interception point can be determined from the two-tone test.

3.2 Two-Tone Signal

When the input signal is composed of more than one frequency component, that is a multi-tone signal, a new type of distortion will occur. In this case, a new set of spectral components will be generated, in addition to those generated by the nonlinearity on each component considered separately. Such components are called the mixing products or more commonly *intermodulation products*. Power series analysis helps in this case in understanding the nonlinear effects of PAs on pass-band communications signals used in real applications. One of the simplest multi-tone tests is the two-tone test, which consists of driving the PA by a two-tone excitation signal, the sum of two sinusoids

$$x(t) = A_1 \cos(2\pi f_1 t + \varphi_1) + A_2 \cos(2\pi f_2 t + \varphi_2). \quad (17)$$

As in section 3.1, the analysis in this paragraph is established in the frequency domain. For simplicity, we assume that the two sinusoids are of equal amplitude ($A_1 = A_2 = A$) and null phases ($\varphi_1 = \varphi_2 = 0$). The Fourier transform of (17) may be written as

$$X(f) = X_{f_1}(f) + X_{f_2}(f) \quad (18)$$

where $X_{f_1}(f)$ and $X_{f_2}(f)$ are the Fourier transforms of the first and second sinusoids in (17), respectively. Substituting (18) in (2), the Fourier transform of the output signal may be written as

$$Y_a(f) = \sum_{k=1}^{K_a} a_k \sum_{i=0}^k \binom{k}{i} \prod_{*}^{k-i} X_{f_1}(f) * \prod_{*}^i X_{f_2}(f). \quad (19)$$

In this summation, for $i = 0$ and $i = k$ (for all values of k) we obtain the responses of the PA for one-tone excitations at frequencies f_1 and f_2 , respectively. In order to compute the term $\prod_{*}^{k-i} X_{f_1}(f) * \prod_{*}^i X_{f_2}(f)$, the following relationship can be used

$$\prod_{*}^{n_1} X_{f_1}(f) * \prod_{*}^{n_2} X_{f_2}(f) = \left(\frac{A}{2}\right)^{n_1+n_2} \sum_{i_1=0}^{n_1} \sum_{i_2=0}^{n_2} \binom{n_1}{i_1} \binom{n_2}{i_2} \delta(f + (n_1 - 2i_1)f_1 + (n_2 - 2i_2)f_2) \quad (20)$$

where $\prod_{*}^0 X_{f_i}(f) = \delta(f)$ and $n_1, n_2 \in N$. Hence, equation (19) can be rewritten in the form

$$Y_a(f) = Y_{f_1}(f) + Y_{f_2}(f) + \sum_{k=2}^{K_a} a_k \left(\frac{A}{2}\right)^k \sum_{i=1}^{k-1} \sum_{i_1=0}^{k-i} \sum_{i_2=0}^i \binom{k}{i} \binom{k-i}{i_1} \binom{i}{i_2} \delta(f + (k - i - 2i_1)f_1 + (i - 2i_2)f_2) \quad (21)$$

where $Y_{f_1}(f)$ ($Y_{f_2}(f)$, respectively) is the Fourier transform of the output signal of the PA when excited by a one-tone signal at the frequency f_1 (f_2 , respectively), that is components at f_1 , f_2 , and their harmonics. However, the third term on the right hand side of Eq. (21) contains a new set of components in addition to those generated by one-tone excitation. These components are the Intermodulation Products (IMPs), and are located around f_1 , f_2 and their harmonics. To illustrate, Fig. 4 shows the output spectrum of the ZHL-100W-52 PA, modeled by an odd order power series, and excited by a two-tone signal. We observe that IMPs appear only around odd order harmonics. In fact, even order harmonics and IMPs around them do not appear because even order terms have been neglected in the adopted polynomial model. This choice does not affect our analysis because, in communication systems, we are generally concerned with IMPs around the fundamental frequencies, as they cannot be easily rejected by filters. Even order IMPs usually occur at frequencies well above or below the fundamentals, and thus are often of little concern.

The two-tone signal is in fact constituted by two amplitude modulated quadrature carriers. Eq.(17) may be written in the form

$$x(t) = \{A_1 \cos(2\pi f_m t - \varphi_1) + A_2 \cos(2\pi f_m t + \varphi_2)\} \cos(2\pi f_c t) - \{A_1 \sin(2\pi f_m t - \varphi_1) - A_2 \sin(2\pi f_m t + \varphi_2)\} \sin(2\pi f_c t) \quad (22)$$

where $f_m = \frac{1}{2}(f_2 - f_1)$ ($f_2 > f_1$) and the carrier frequency $f_c = \frac{1}{2}(f_1 + f_2)$. In the particular case where $A_1 = A_2 = A$ and $\varphi_1 = \varphi_2 = 0$, Equation (22) is written

$$x(t) = 2A \cos(2\pi f_m t) \cos(2\pi f_c t). \quad (23)$$

The two-tone signal used is, hence, an amplitude modulated carrier.

The components in (21), $\delta(f + (k - i - 2i_1)f_1 + (i - 2i_2)f_2)$, can be expressed in function of f_c and f_m , $\delta(f + (k - 2(i_1 + i_2))f_c - (k - 2i - 2i_1 + 2i_2)f_m)$. So, as mentioned before, only odd-degree terms generate components in the vicinity of f_c (i.e. the vicinity of f_1 and f_2), since the

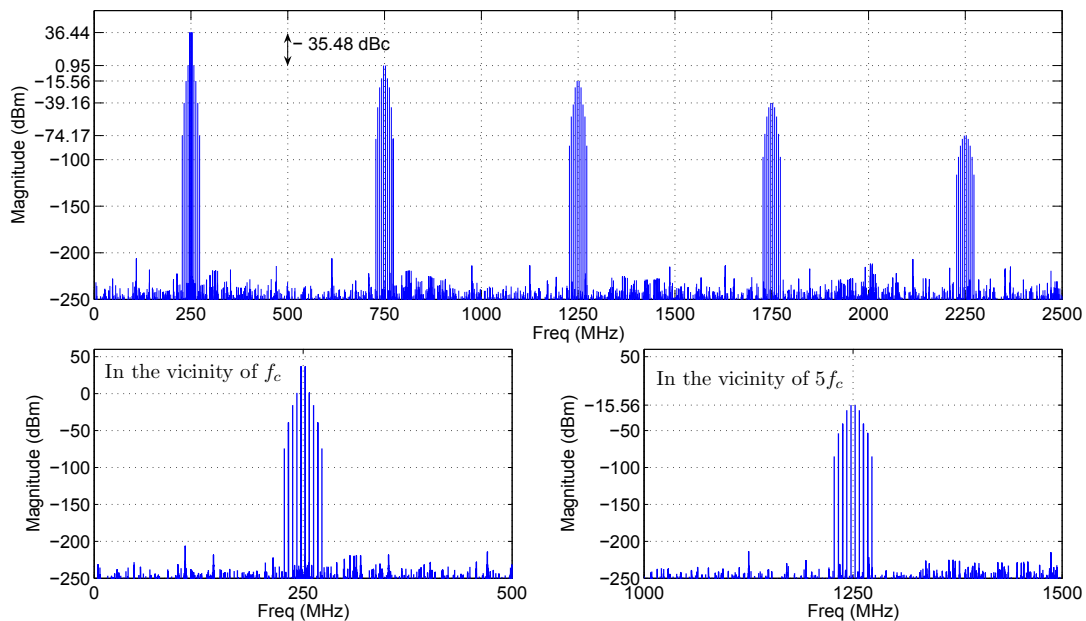


Fig. 4. Output spectrum of the ZHL-100W-52 PA, modeled by a 9^{th} -order polynomial model with odd degree terms only, and excited by a two-tone signal ($P_{avg}^{in} = -7$ dBm)

condition $k - 2(i_1 + i_2) = \pm 1$ must be verified. The set of components in the vicinity of $+f_c$ can be extracted from (21) to form the following equation

$$Y_a(f) \Big|_{+f_c} = \sum_{k=1}^K a_{2k-1} \left(\frac{A}{2}\right)^{2k-1} \sum_{i=0}^{2k-1} \sum_{\substack{i_1=k-i \\ 2k-i-1 \geq i_1 \geq 0}}^k \binom{2k-1}{i} \binom{2k-i-1}{i_1} \binom{i}{k-i_1} \delta(f - f_c - (4k - 2i - 4i_1 - 1)f_m). \quad (24)$$

Note that the components at frequencies $f_1 = f_c - f_m$ and $f_2 = f_c + f_m$ are included in (24). Similarly to the one tone test, we are interested here in analyzing the nonlinearity on all the components close to f_c when sweeping the input power level on a finite range of power. In the following, we discuss the nonlinearity on the fundamental components and provide a new definition of interception points.

3.2.1 AM/AM Characteristic

In a two-tone test the AM/AM characteristic is often not determined, and no related parameters are given in the data sheet of the power amplifier. However, it is often advantageous to determine the amount of nonlinearity on the two fundamental components w.r.t the nonlinearity on the unique fundamental component in the one-tone test. Therefore, the AM/AM characteristic of the two-tone test will be determined by measuring the output power at the two fundamentals, f_1 and f_2 , for different values of the average input power (i.e., the input power at the two fundamental components). Every term in (24), generates one or more frequency components at $+f_1$ and $+f_2$. To illustrate, let us take the sum of all frequency

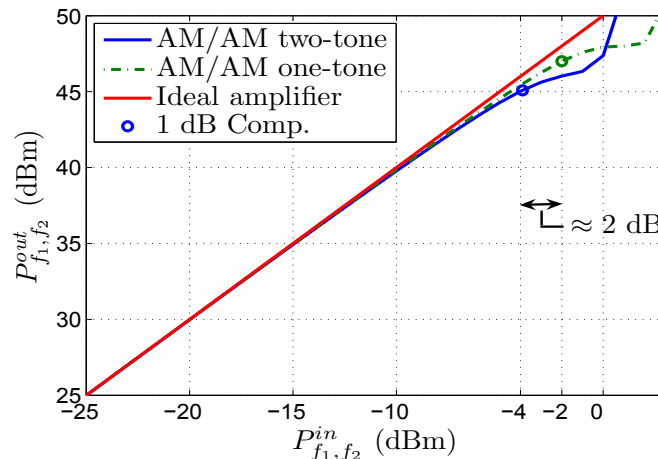


Fig. 5. AM-AM characteristics: one- and two-tone excitation signals

components at $+f_2 = f_c + f_m$

$$Y_a(+f_2) = \sum_{k=1}^K a_{2k-1} \left(\frac{A}{2}\right)^{2k-1} \sum_{i=1}^k \binom{2k-1}{2i-1} \binom{2(k-i)}{k-i} \binom{2i-1}{i-1}. \quad (25)$$

The output power, P_{f_1, f_2}^{out} , at the two frequencies f_1 and f_2 , can be determined from (25), if we exploit the symmetry of the spectrum around the origin $f = 0$ and the symmetry of IMPs close to f_1 and f_2 around the carrier frequency f_c

$$P_{f_1, f_2}^{out} = 10 \log_{10} \frac{4 |Y_a(+f_2)|^2}{R 10^{-3}} \quad (26)$$

Similarly to (9), this power can be expressed in the form

$$P_{f_1, f_2}^{out} = P_{f_1, f_2}^{in} + G + Gc_{f_1, f_2} \quad (27)$$

where

$$Gc_{f_1, f_2} = 10 \log_{10} (1 + S)^2, \quad (28)$$

$S = \sum_{k=2}^K \frac{a_{2k-1}}{a_1} (A/2)^{2(k-1)} \sum_{i=1}^k C_{2k-1}^{2i-1} C_{2(k-i)}^{k-i} C_{2i-1}^{i-1}$ and G is the gain of the PA (10). The input power at f_1 and f_2 , P_{f_1, f_2}^{in} is equal to $10 \log_{10} \left(\frac{4 |X(+f_2)|^2}{R 10^{-3}} \right)$, which is equal to the average input power P_{avg}^{in} . For values of i equal to k in the summation of equation (28), we get the summation S of (11). Denoting it by S_1 , Eq.(28) can be expressed in the form

$$Gc_{f_1, f_2} = 10 \log_{10} (1 + S_1 + S_2)^2 \quad (29)$$

where $S_2 = \sum_{k=2}^K \frac{a_{2k-1}}{a_1} (A/2)^{2(k-1)} \sum_{i=1}^{k-1} C_{2k-1}^{2i-1} C_{2(k-i)}^{k-i} C_{2i-1}^{i-1}$.

According to Eq. (29), the gain compression on the two fundamental components of the two-tone signal is faster than the gain compression on the unique component of the one-tone signal, as shown in figure 5. The compression region in this case is shifted down and consequently the 1dB compression point is backed off.

In order to interpret this phenomenon, a number of parameters are needed. As already mentioned, a two-tone signal is a varying envelope signal (23). Two parameters are often used to characterize this type of signals (Cripps, 2006):

- The *PEP* (Peak Envelope Power), P_{peak} , often measured in dBm and defined by

$$P_{peak} = 10 \log_{10} \frac{(A_{peak}/\sqrt{2})^2}{R10^{-3}} \text{ (dBm)}$$

where A_{peak} is the peak amplitude of the signal (equal to $2A$ in the case of a two-tone signal).

- The *PAPR* (Peak-to-Average Power Ratio), which is the ratio between the PEP and the average power of the signal. It is therefore the difference in dB between the PEP and the average power P_{avg} expressed both in dBm, $PAPR = P_{peak} - P_{avg}$ (dB)

In the case of a two-tone signal, a deterministic signal, the PAPR is equal to 3 dB ($P_{peak} = P_{avg} + 10 \log_{10} 2$).

Other parameters are also used in order to locate the input/output signal w.r.t the AM/AM characteristic of the PA².

- The *IPBO* (Input Peak Backoff), which is the difference in dB between the input saturation power of the PA P_{sat}^{in} and the peak power P_{peak}^{in} of the input signal, $IPBO = P_{sat}^{in} - P_{peak}^{in}$ (dB). Similarly, the *Output Peak Backoff* (OPBO) is given by $OPBO = P_{sat}^{out} - P_{peak}^{out}$ where P_{sat}^{out} is the output saturation power of the PA and P_{peak}^{out} is the peak power of the output signal.
- The *IBO* (Input Backoff), which is the difference in dB between P_{sat}^{in} and the average input power P_{avg}^{in} , $IBO = P_{sat}^{in} - P_{avg}^{in}$ (dB). Similarly, the *Output Backoff* (OBO) is given by $OBO = P_{sat}^{out} - P_{avg}^{out}$.

To this we add a last definition, which is the instantaneous power of a signal $x(t)$, $P_{inst}(t)$ expressed in dBm

$$P_{inst}(t) = 10 \log_{10} \frac{(x(t)/\sqrt{2})^2}{R10^{-3}} \quad (30)$$

Let us consider, now, the particular case when the gain compression on the fundamental components of the two-tone signal is equal to 1 dB. Referring to Fig. 5, the average input power P_{avg}^{in} causing this amount of gain compression is approximately equal to -4 dBm. For this same P_{avg}^{in} value, we observe that the compression on the fundamental component of the one-tone signal is less than 1 dB. Thus, we can conclude that the gain compression is related to the instantaneous input power rather than the average input power.

If we interpret this by considering a discrete representation of the signals, we can conclude that some samples of the two-tone signal can undergo gain compression bigger than 1 dB since its P_{peak}^{in} exceeds the 1 dB compression point. On the other hand, the samples of the one-tone signal, which is a non-varying envelope signal, take always values less than its average power, which is equal to its P_{peak}^{in} . This interpretation is better illustrated in Fig. 6, where the

² Note that when we talk about the AM/AM characteristic without specifying the signal used to extract it, we designate the one corresponding of a one-tone test.

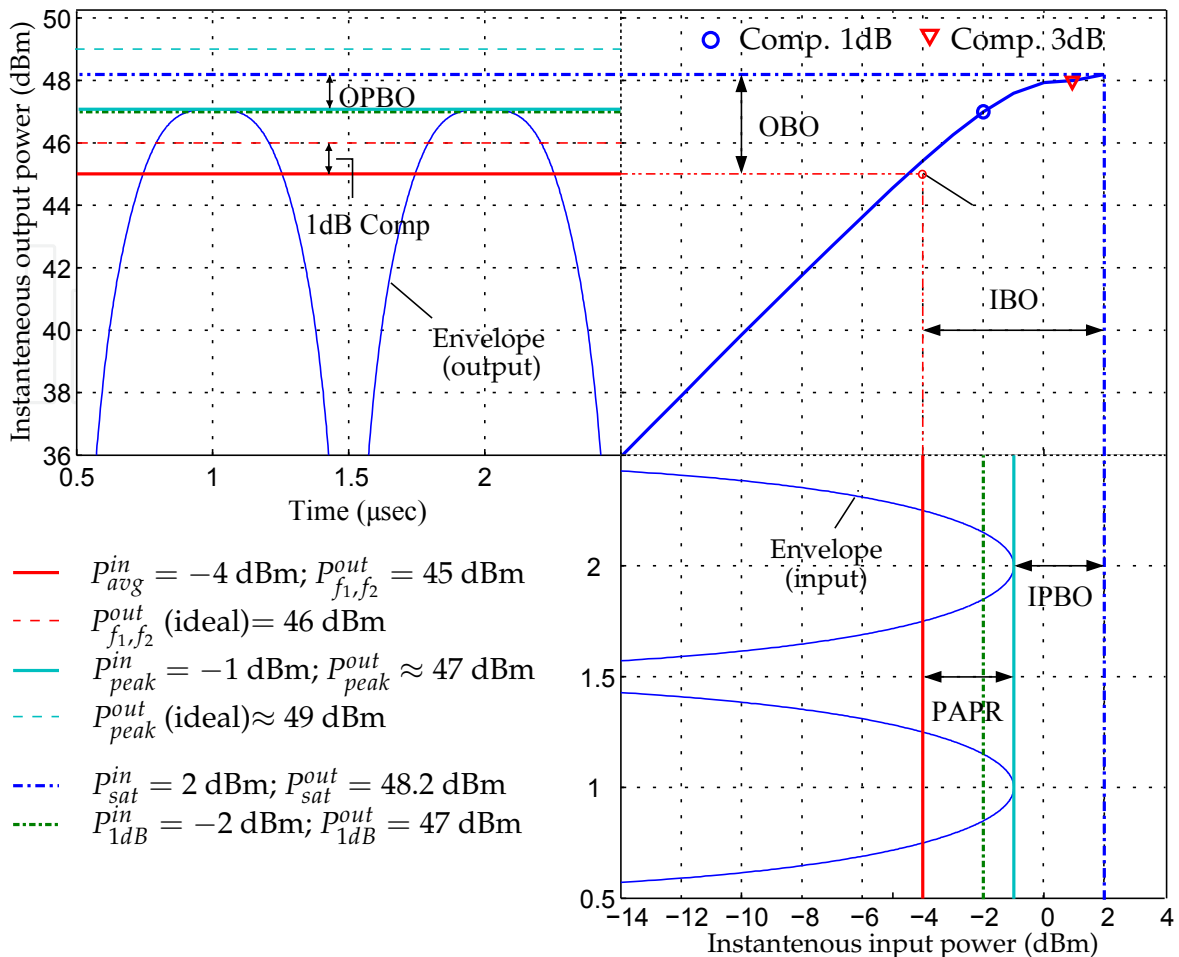


Fig. 6. Input/output envelope variation of a two tone signal with respect to AM/AM characteristic

instantaneous power of the input/output two-tone envelope signals are presented in comparison with the AM/AM characteristic. All the parameters already defined are also shown on this figure (Fig. 6), for this particular case. Therefore, we conclude that the envelope variation of the two-tone signal makes it more vulnerable to nonlinearity.

Besides, it is important to note that for varying envelope signals, it is very difficult to predict or to quantify the amount of gain compression at the output of the PA (the OBO and OPBO values), even in the case of deterministic signals like the two-tone signal. This is due to the fact that various parameters and nonlinear relations are involved.

In general, reducing the nonlinear distortion is at the expense of power efficiency. In fact, the power efficiency of the PA is likely to increase when its operating point approaches the saturation. But, for all the reasons already mentioned, and in order to preserve the form of the envelope of the input signal, large power backoffs are classically imposed. For an ideal amplification, the IPBO must be sufficiently important to prevent the envelope from penetrating the compression region. Doing so the power efficiency of the PA decreases considerably, especially if the input signal has a high PAPR value. In the second part of this chapter, we will present an important technique used to resolve this problem.

3.2.2 Interception Points

In the one-tone test, the n^{th} interception point was determined as the input (output) power level for which the fundamental frequency component and the n^{th} harmonic have the same output power level. In a two-tone test we are interested to the power levels of the odd-order IMPs close to the fundamental frequencies (f_1 and f_2). Due to the symmetry of these IMPs around f_c^3 , we will consider below the products at the right side of $+f_c$ only, that is at the frequencies $f_c + (2m - 1)f_m$ where $m = 1, 2, \dots$. Every term in the summation (24) having an odd-degree equal or greater than $2m - 1$, generates a spectral component at the frequency $f_c + (2m - 1)f_m$. Depending on the value of m , the sum of all the components can be expressed by one of the two following forms. Equation (31) corresponds to even values, while equation (32) corresponds to odd values

$$Y_a(f_c + (2m - 1)f_m) = \sum_{k=m}^K a_{2k-1} \left(\frac{A}{2}\right)^{2k-1} \sum_{i=\frac{m}{2}}^{k-\frac{m}{2}} \binom{2k-1}{2i} \binom{2k-1-2i}{k-i+\frac{m}{2}-1} \binom{2i}{i-\frac{m}{2}} \quad (31)$$

$$Y_a(f_c + (2m - 1)f_m) = \sum_{k=m}^K a_{2k-1} \left(\frac{A}{2}\right)^{2k-1} \sum_{i=\frac{m+1}{2}}^{k-\frac{m-1}{2}} \binom{2k-1}{2i-1} \binom{2(k-i)}{k-i+\frac{m-1}{2}} \binom{2i-1}{i-\frac{m+1}{2}}. \quad (32)$$

Note that for $m = 1$, Eq. (32) is equivalent to Eq. (25). The output power of any of those IMPs can be determined from equations (31) and (32). For even values of m , the power of the $(2m - 1)^{\text{th}}$ IMP, may be expressed (similarly to (14)) in function of the average input power $P_{\text{avg}}^{\text{in}} = P_{f_1, f_2}^{\text{in}}$, or in function of the power of one of the two fundamental components, $P_{f_1}^{\text{in}}$ or $P_{f_2}^{\text{in}}$. The latter relation is the more commonly used and we will adopted hereafter,

$$P_{\text{IMP}_{2m-1}}^{\text{out}} = (2m - 1)P_{f_1}^{\text{in}} + G_{\text{IMP}_{2m-1}} + G_{c\text{IMP}_{2m-1}} \quad (33)$$

where

$$G_{\text{IMP}_{2m-1}} = 10 \log_{10} (C_{2m-1}^m a_{2m-1})^2 - 32(m - 1), \quad (34)$$

$$G_{c\text{IMP}_{2m-1}} = 10 \log_{10} (1 + S)^2 \quad (35)$$

and $S = \sum_{k=m+1}^K \frac{a_{2k-1}}{a_{2m-1}} \left(\frac{A}{2}\right)^{2(k-m)} \sum_{i=\frac{m}{2}}^{k-\frac{m}{2}} C_{2k-1}^{2i} C_{2k-1-2i}^{k-i+\frac{m}{2}-1} C_{2i}^{i-\frac{m}{2}}$. For odd values of m , only the summation in equation (35) will change, and becomes in this case, $S = \sum_{k=m+1}^K \frac{a_{2k-1}}{a_{2m-1}} \left(\frac{A}{2}\right)^{2(k-m)} \sum_{i=\frac{m+1}{2}}^{k-\frac{m-1}{2}} C_{2k-1}^{2i-1} C_{2(k-i)}^{k-i+\frac{m-1}{2}} C_{2i-1}^{i-\frac{m+1}{2}}$. Note that in (33), $P_{f_1}^{\text{in}}$ is equal to $P_{\text{avg}}^{\text{in}} - 3 \text{ dB}$.

Hence, the IMPs, like the fundamental components, undergo gain compression. For low input power levels, the gain compression is negligible. In this range of power, the output power of the $(2m - 1)^{\text{th}}$ product, $P_{\text{IMP}_{2m-1}}^{\text{out}}$, $m = 1, 2, \dots$, increase linearly in function of $P_{f_1}^{\text{in}}$ (33). However, this evolution is $2m - 1$ times faster than the power at one of the fundamental frequencies, if taken separately (one-tone test, Eq. (9)). Therefore, if the gain compression phenomenon does not occur, one could expect an input (output) power level, for which, the $(2m - 1)^{\text{th}}$ IMP and one of the fundamental components will have the same power level. In this case, The input (output) power level is called the $(2m - 1)^{\text{th}}$ input (output) interception

³The symmetry of IMPs around f_c is related to the memoryless assumption.

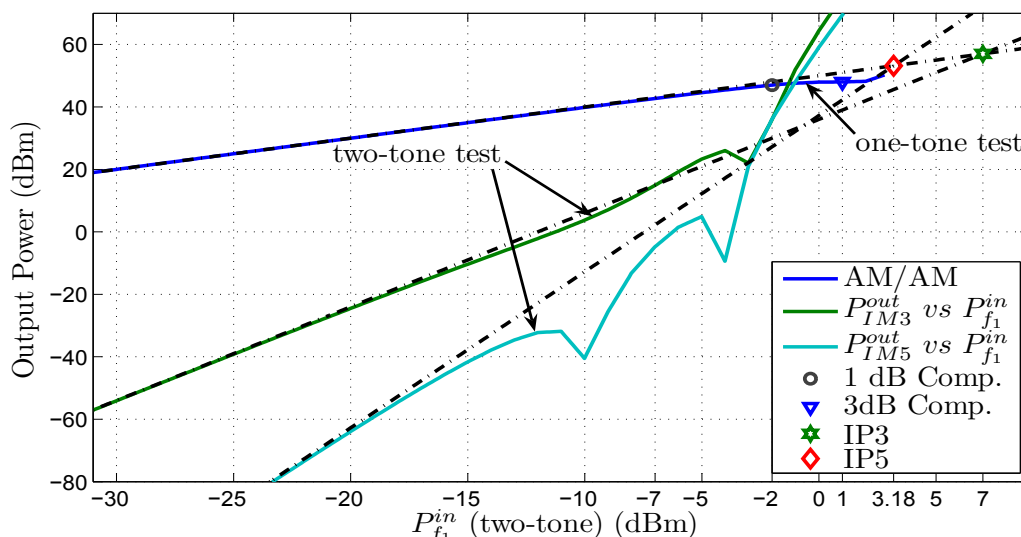


Fig. 7. 1 and 3dB compression points, and third and fifth interception points

point, denoted IP_{2m-1}^{in} (IP_{2m-1}^{out}). This point is thus the interception point of the linear extrapolations of power evolution curves (9) and (33). This new definition of the interception point is often preferred to the first one (Section 3.1), since it gives an indication on the amount of spectral regrowth in real applications, when the PA is excited by a band-pass signal (Sec. 3.3). Figure 7 shows the 3rd and 5th interception points, as well as the AM-AM characteristic, and its corresponding compression points for our case-study PA, the ZHL-52-100W. Here, we observe that the power series model is able to describe the nonlinearity on IMPs, only over a limited power range.

3.2.3 Model Identification

Some parameters presented in the preceding sections appear in almost every RF PA data sheet. They are adopted to give a first indication on the nonlinearity of the PA. In this section, we present how such parameters could be used to determine the coefficients a_k of the ZHL-100W-52 9th-order polynomial model, adopted all along our simulations. As mentioned before, even-order terms are neglected, and thus only odd-order coefficients will be identified. Recall that the identified model takes into account nonlinear amplitude distortion only.

The first coefficient of the power series a_1 can be determined simply from the gain of the PA (10), $a_1 = 10^{G/20}$. For the ZHL-100W-52, the gain is equal to 50 dB, and, hence $a_1 = 316.23$. On the other hand, referring to equations (9), (33) and (34), we can write

$$IP_{2m-1}^{in} + G = (2m - 1)IP_{2m-1}^{in} + 10 \log_{10}((C_{2m-1}^m a_{2m-1})^2) - 32(m - 1). \quad (36)$$

Thus, if the $(2m - 1)^{th}$ input interception point is known, IP_{2m-1}^{in} , we can determine the coefficient of the same order, a_{2m-1} of the power series

$$a_{2m-1} = \frac{10^{\frac{32(m-1)+G-2(m-1)IP_{2m-1}^{in}}{20}}}{C_{2m-1}^m}. \quad (37)$$

In our case-study PA, the third interception point at the output is specified, $IP_3^{out} = 57$ dBm, allowing thus to determine the third coefficient a_3 . Note that, given IP_{2m-1}^{out} , IP_{2m-1}^{in} could be

simply obtained by setting Gc_{f_0} to zero in Eq. (9), $IP_{2m-1}^{out} = IP_{2m-1}^{in} + G$, since the interception point is always on the ideal PA characteristic. Thus, a_3 is equal to -837.3 .

Moreover, based on Eq. (36), we could express a_{2m-1} in function of the amplitude corresponding to the $(2m - 1)^{th}$ interception point at the input, $A_{IP_{2m-1}}$, and the coefficient a_1

$$a_{2m-1} = \frac{a_1}{C_{2m-1}^m (A_{IP_{2m-1}}/2)^{2(m-1)}}. \quad (38)$$

In traditional power series analysis, the order of the used model is usually limited to 3. Thus, we can determine a relation between A_{1dB} and A_{IP3} , which correspond to the 1 dB compression point (one-tone test), and the third interception point (two-tone test), respectively. Here, if we set Gc_{f_0} in 11, we find the following relation

$$A_{1dB}^2 = \frac{4a_1(10^{-1/20} - 1)}{3a_3}. \quad (39)$$

Note that, the coefficient a_3 should have, in this case, a negative value in order to model the gain compression of the PA. Now, substituting a_3 from (38), in Eq. (39), we obtain a new relation between A_{1dB} and A_{IP3}

$$\left(\frac{A_{1dB}}{A_{IP3}}\right)^2 = 1 - 10^{-1/20}. \quad (40)$$

Eq. (40) and Eq. (38) for $m = 2$, could be found in almost all classical studies on modeling the PA via power series (e.g. chap. 9, (Cripps, 2006)).

Now, thanks to Eq. (11) obtained from our development, every point of the AM/AM characteristic can be used to determine a new higher-order coefficient. For example, two compression points are given in the data sheet of the ZHL-100W-52 PA, and a third point near saturation could be deduced since the maximum input power is specified (Maximum Input power no damage) and is equal to 3 dBm. Hence, we can choose for example an additional point at 2 dBm input power with a compression greater than 3 dB, let us say 3.8 dB and we suppose that this point is the saturation of the PA. We have added this point to reinforce the modeling capacity of the power series model by extending its power range validity (in other words, delaying its divergence point) and to define a saturation point useful for the development in this chapter (Fig. (6)). Finally, setting Gc_{f_0} to -1 , -3 , and -3.8 successively, a linear system of three equations with three unknowns can be established. In a matrix notation, this system can be written

$$\mathbf{C}\mathbf{x} = \mathbf{b} \quad (41)$$

where $\mathbf{C}^T = [v_{1dB} \ v_{3dB} \ v_{3.8dB}]$, $\mathbf{v}_{pdB}^T = [C_5^3(A_{pdB}/2)^4 \ C_7^4(A_{pdB}/2)^6 \ C_9^5(A_{pdB}/2)^8]$, $\mathbf{x}^T = [a_5 \ a_7 \ a_9]$ et $\mathbf{b}^T = [u_{1dB} \ u_{3dB} \ u_{3.8dB}]$ where $u_{pdB} = a_1(10^{-p/20} - 1) - a_3 C_3^2(A_{pdB}/2)^2$, $(\cdot)^T$ being the transpose operator. The solution of this linear system (41) can be simply written

$$\mathbf{x} = \mathbf{C}^{-1}\mathbf{b}. \quad (42)$$

If the matrix \mathbf{C} is not singular, we can find an exact unique solution of (42), and otherwise the least square method can be used. The founded values of a_5 , a_7 et a_9 for the ZHL-100W-52, are respectively 11525.2, -224770 and 952803.3. Note that, we can exploit all the power points of the measured AM-AM characteristic to identify more coefficients and to improve the least square method accuracy.

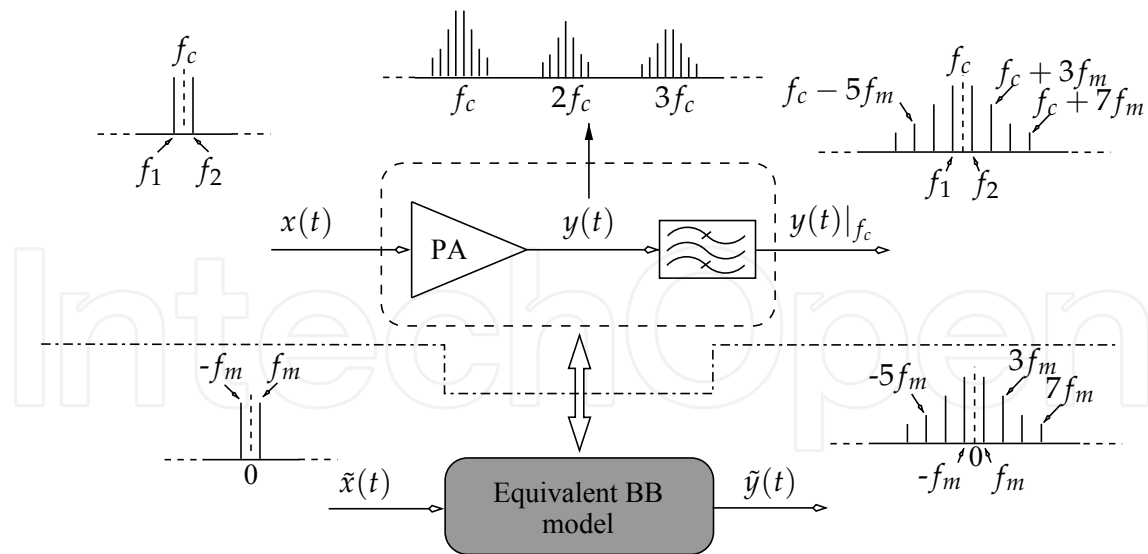


Fig. 8. Equivalent baseband modeling of the PA

3.3 Band-pass signals and baseband equivalent Modeling

So far, we have discussed the nonlinearity on one- and two-tone signals. However, in real modern communications systems, more complex signals are used to transmit digital information by some type of carrier modulation. Besides, due to bandwidth constraints, narrowband *band-pass* signals are generated in most applications. Signals are termed narrowband band-pass signals or, shortly, band-pass signals, when they satisfy the condition that their bandwidth is much smaller than the carrier frequency. Such a signal can be expressed by

$$\begin{aligned} x(t) &= \Re \left\{ \tilde{x}(t) e^{j2\pi f_c t} \right\} \\ &= \frac{1}{2} \left(\tilde{x}(t) e^{j2\pi f_c t} + \tilde{x}^*(t) e^{-j2\pi f_c t} \right) \end{aligned} \quad (43)$$

where f_c is the carrier frequency and $\tilde{x}(t)$ is the complex envelope of the signal or the *baseband* signal. Substituting (43) into Eq. (1), and using the binomial theorem, the output signal of the PA modeled by a power series model can be written

$$\begin{aligned} y_a(t) &= \sum_{k=1}^{K_a} a_k \frac{1}{2^k} \left(\tilde{x}(t) e^{j2\pi f_c t} + \tilde{x}^*(t) e^{-j2\pi f_c t} \right)^k \\ &= \sum_{k=1}^{K_a} a_k \frac{1}{2^k} \sum_{i=0}^k \binom{k}{i} \tilde{x}^i(t) \tilde{x}^{*(k-i)}(t) e^{j2\pi(2i-k)f_c t}. \end{aligned} \quad (44)$$

In the above equation, only odd-degree terms generate frequency components close to f_c , since the condition $i = (k \pm 1)/2$ must be verified. The sum of all these components, denoted $y_a(t)|_{f_c}$, can be extracted from (44) to form the following equation

$$\begin{aligned} y_a(t)|_{f_c} &= \sum_{k=1}^K a_{2k-1} \frac{1}{2^{2k-1}} C_{2k-1}^k |\tilde{x}(t)|^{2(k-1)} \left(\tilde{x}^*(t) e^{-j2\pi f_c t} + \tilde{x}(t) e^{j2\pi f_c t} \right) \\ &= \sum_{k=1}^K a_{2k-1} \frac{1}{2^{2(k-1)}} C_{2k-1}^k |\tilde{x}(t)|^{2(k-1)} x(t). \end{aligned} \quad (45)$$

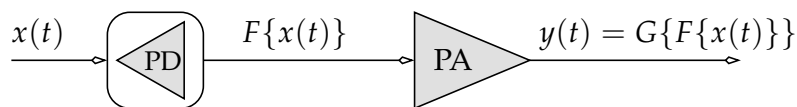


Fig. 9. Predistortion technique

Since we are interested only by the frequency content near f_c , this result (45) suggests that it is sufficient to study the nonlinearity of the PA on the complex envelope of the input signal. Denoting by $\tilde{y}(t)$ the complex envelope of the output signal (44) filtered by a band-pass filter centered on f_c , Eq. (45) can be written

$$\tilde{y}(t) = \sum_{k=1}^K a'_{2k-1} |\tilde{x}(t)|^{2(k-1)} \tilde{x}(t) \quad (46)$$

where $a'_{2k-1} = a_{2k-1} \frac{1}{2^{2(k-1)}} C_{2k-1}^k$ (Benedetto & Biglieri, 1999). Eq. (46) constitutes a baseband equivalent model of the RF power series model (1) used before. The baseband model is in fact valid in all cases where band-pass signals are used. It is particularly interesting for digital simulators since baseband signals require relatively low sampling rate w.r.t the carrier frequency. In addition to its capacity of representing simply power amplifiers, this model is often used in baseband predistortion techniques, when the PA does not represent strong memory effects. To illustrate, the baseband signal of a two-tone signal, which can be considered as a band-pass signal, is a sinusoidal signal $\tilde{x}(t) = 2A \cos(2\pi f_m t)$ (Eq. (23)), and the equivalent baseband system is illustrated in Fig. 8.

As mentioned before, a memoryless nonlinear system can induce amplitude distortion only, but never phase distortion. However, PAs with weak memory effects can be considered as quasi-memoryless systems (Bosch & Gatti, 1989), where nonlinear amplitude and phase distortion at instant t depend only on the amplitude of the input envelope signal at the same instant. Hence, the output complex envelope can be expressed in the general form

$$\begin{aligned} \tilde{y}(t) &= G(|\tilde{x}(t)|) \tilde{x}(t) \\ &= G_a(|\tilde{x}(t)|) \exp\{j\Phi(|\tilde{x}(t)|)\} \tilde{x}(t) \end{aligned} \quad (47)$$

where $G_a(\cdot)$ and $\Phi(\cdot)$ are nonlinear functions of the amplitude, $|\tilde{x}(t)|$, of the input complex envelope. The equivalent baseband power series model (46) can be used to describe the behavior of a quasi-memoryless system, and it is often called the quasi-memoryless polynomial (QMP) model. In this case, the coefficients a'_{2k-1} are complex valued, and from (46), the complex gain G of the PA (47) is equal to $\sum_{k=1}^K a'_{2k-1} |\tilde{x}(t)|^{2(k-1)}$. In this modeling approach, the nonlinear functions $G_a(\cdot)$ and $\Phi(\cdot)$, which are the module and the phase of the complex gain of the PA respectively, represent the AM/AM et AM/PM conversions of the PA.

In the next part of this chapter, a digitally modulated signal (a band-pass signal) is used while evaluating a linearization technique. Thus, we will observe the nonlinear effects that can be incurred by the PA on such a type of signals.

4. Adaptive digital baseband predistortion technique

Linearization techniques aim to linearize the behavior of the PA in its nonlinear region, or to extend the linear behavior over its operating power range. Generally speaking, this can be done by acting on the input and/or output signals without changing the internal design of

the PA. Two linearization techniques were first applied to PAs, both invented by H. S. Black (Black, 1928; 1937): the Feedback (FB) and Feedforward (FF) techniques. Different implementation approaches have been proposed in the literature but the main idea behind these techniques is to generate a corrective signal by comparing the distorted output signal to the input signal, and to combine it either to the input (FB) or output signal (FF). The FB technique, as any feedback system, suffers from instability problems which limit its deployment to narrow-band applications. On the other hand, FF technique is inherently an open-loop process and, thus, it can be applied to wide-band applications but it has many disadvantages, mainly due to signals combination at the output of the PA. More recently, a new technique, called the predistortion technique, has been proposed and widely used. This technique consists in inserting a nonlinear circuit, the *predistorter* (PD), prior to the RF PA such that the combined transfer characteristic of both is linear (Fig. 9). Denoting by G and F the transfer characteristic of the PA and the PD respectively, the output signal $y(t)$ of the cascade of the two circuits, PA and PD, may be written

$$y(t) = G \{F \{x(t)\}\} = Kx(t) \quad (48)$$

where K is a positive constant representing the gain of the linearized PA, and $x(t)$ is the input signal. Different approaches, relying on analog, digital or hybrid circuits, could be employed while designing the PD. In the following, however, we will be interested in Adaptive Digital Predistortion (ADPD), which is a promising and cost-effective technique for SDR transmitters. Given the considerable processing power now available from Digital Signal Processing (DSP) devices, the digital implementation offers high precision and flexibility.

4.1 ADPD: An overview

The digital predistortion technique is basically relying on the equivalent baseband modeling of the PA and/or its inverse. For digital signal processing convenience, it is very desirable to implement the PD in baseband. To this end, we resort to an equivalent low-pass or baseband representation of the band-pass system. Thus, the cascade of the equivalent baseband behavioral model of the PD and the PA should form a global linear system, as shown in figure 10. Hereafter, F and G will represent the transfer characteristic at baseband of the PA and the PD respectively. To illustrate, we will assume that the PD and the PA are quasi-memoryless systems, and thus G and F are nonlinear functions of the amplitude of their input signals. Hence, the output $x_p(t)$ of the PD can be written in function of the input signal $x_i(t)$ as follows

$$x_p(t) = F(|x_i(t)|)x_i(t) \quad (49)$$

Accordingly, the output of the PA is written as

$$\begin{aligned} y(t) &= G(|x_p(t)|)x_p(t) \\ &= G(|F(|x_i(t)|)x_i(t)|)F(|x_i(t)|)x_i(t) \\ &= G_{lin}(|x_i(t)|)x_i(t) \end{aligned} \quad (50)$$

where $y(t)$ is the output baseband signal and $G_{lin}(\cdot)$ the characteristic function of the linearized PA, LPA (i.e. cascade of the PA and the PD). In an ideal scenario, the module and phase of this function must be constant for the whole amplitude range up to saturation. Thus, according to Eq. (50), a linear behavior can be obtained if the following condition is fulfilled

$$|G(|x_p(t)|)F(|x_i(t)|)| = K \quad (51)$$

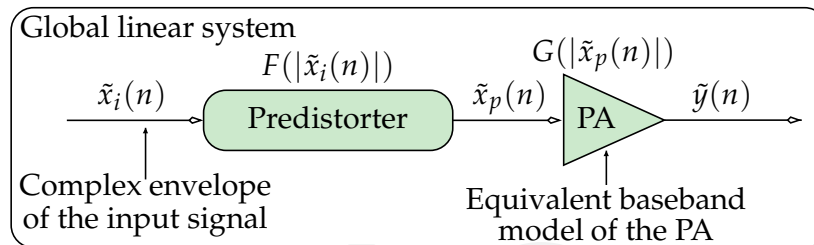


Fig. 10. Baseband predistortion

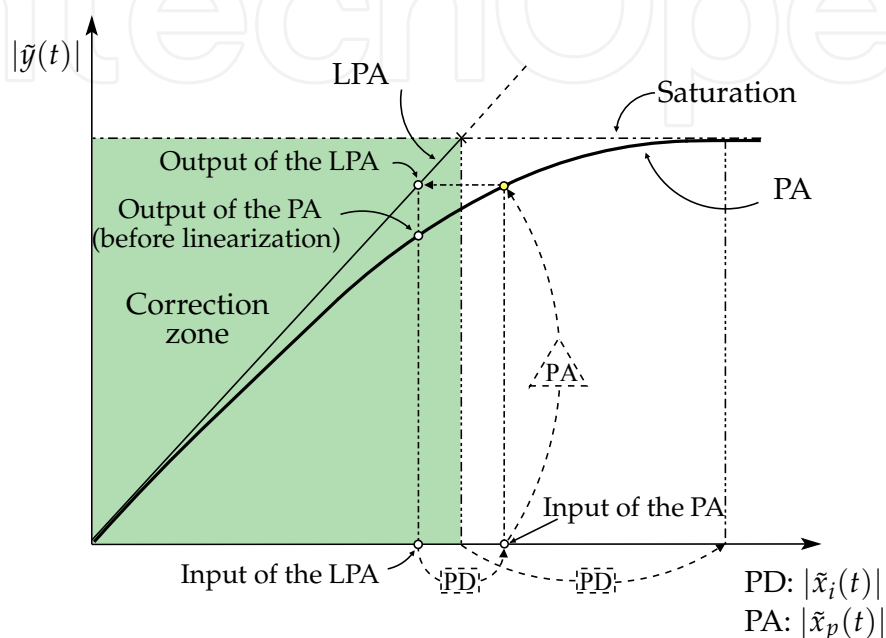


Fig. 11. Instantaneous amplitude predistortion

where K , a positive constant, is the global gain of the LPA. For further illustration, Fig. 11 shows the instantaneous predistortion mechanism in the simple case where the PA introduces amplitude distortion only. The insertion of the PD makes linear the amplitude response of the PA over a large amplitude range, covering part of the compression zone, before reaching saturation. A phase predistortion should be also performed since the phase distortion of the PA has considerable effects on the output signal.

There are different configurations of the digital baseband predistortion system. However, all these configurations have the same principle presented in Fig. 12. The transmitted RF signal at the output of the PA is converted to baseband, and its quadrature components are digitized by an analog to digital converter. The samples in baseband are then treated by a digital signal processor (DSP) with an algorithm that compares them to the corresponding samples of the reference input signal. The PD's parameters are identified while trying to minimize the error between the input and the output, or another appropriate cost function. After a short time of convergence which characterizes the identification algorithm, the PD could perform as the exact pre-inverse of the equivalent baseband model of the PA.

In modern SDR transmitters, most of the components must be reconfigurable in order to switch, ideally on the fly, from one standard to another. In such systems, the digital predistortion technique seems to be the unique applicable linearization technique. In this case,

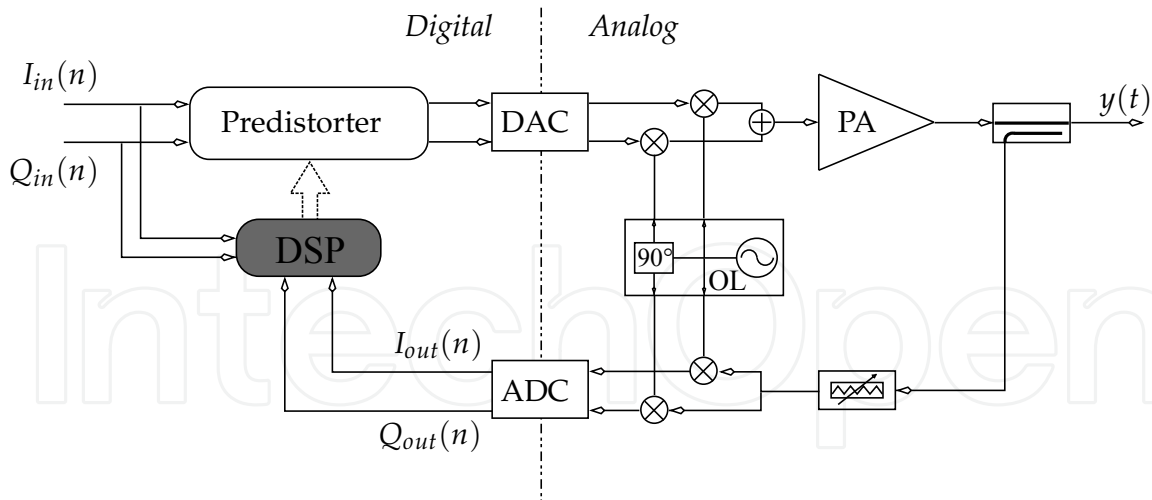


Fig. 12. Adaptive digital baseband predistortion

the PD must be updated on a continuous or quasi-continuous basis in order to keep a good linearization performance, and thus the lowest energy dissipation.

4.2 Performance evaluation

In this section, we first describe the test bench designed for our experiments. Then, we evaluate the performance of the digital baseband predistortion technique, using a medium power PA from Mini-Circuits, the ZFL-2500, driven by 16-QAM modulated signal. To this end, we first identify a model of this PA from the input/output signals acquired using the test bench. This model is used in simulations to determine the best expected performance of the digital baseband predistortion technique, in the ideal scenario (without measurement noise). Second, we present the experimental results, and compare them to the theoretical ones. The performance of the PD has been evaluated by measuring two important parameters, the Adjacent Channel Power Ratio (ACPR) and Error Vector Magnitude (EVM), for different backoff values. However, due to space limitation, we will only present the results obtained for the ACPR parameter.

4.2.1 Test bench description

The measurement testbed consists of a vector signal generator (VSG) and a digital oscilloscope (DO) (Fig. 13). This testbed was designed to be fully automatic using the instrument toolbox of Matlab. The measurement technique concept consists in generating data in Matlab to send out to the VSG and then to read data into Matlab for analysis. The VSG (Rhode & Schwartz SMU 200A) receives the complex envelope data via an Ethernet cable (TCP/IP) from a personal computer (PC) and using a direct up-conversion from baseband to RF, produces virtually any signal within its bandwidth limits. Note that, once the data have been sent to the VSG, the latter will send the corresponding modulated signal repeatedly to the PA. A marker can be activated to trigger the DO every time the sequence is regenerated. The microwave input and output signals of the PA are then sampled simultaneously in the real time oscilloscope (LeCroy, 4 channels Wave master 8600, 6GHz bandwidth, 20 GS/sec), transferred via an Ethernet cable to the PC, and recorded in the workspace of Matlab. The acquisition time in the DO is fixed to be equal to the duration of the baseband signal generated by Matlab. In this way, the acquired RF signals correspond exactly to the original signal of Matlab. After

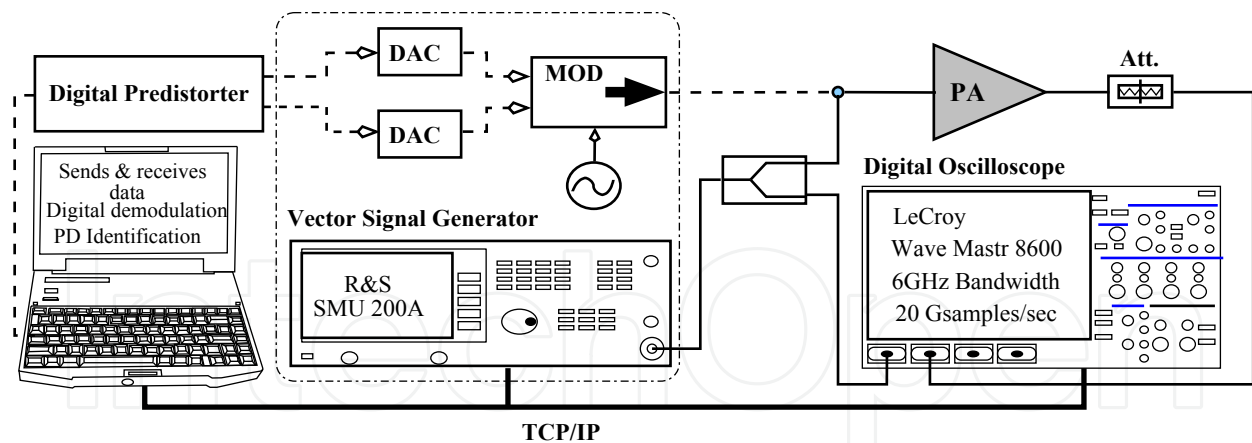


Fig. 13. Measurements setup

that, the two sequences are digitally demodulated in Matlab, adjusted using a subsampling synchronization algorithm (Isaksson et al., 2006), and processed in order to identify the parameters of the PD. The baseband signal is then processed by the predistortion function and loaded again to the VSG. Finally, the output of the linearized PA is digitized in the DO and sent back to the PC to evaluate the performance of the particular PD scheme. This evaluation can be done by comparing the output spectra (ACPR) and constellation distortion (EVM) of the PA with and without linearization, for different back-off values. The time of this entire test is several minutes since this test bench is fully automatic. In other words, the transmission and the signals acquisition, identification and performances evaluation can be implemented in a single program in Matlab which run without interruption. Note that, for signals acquisition, the spectrum analyzer "Agilent E4440A" has been also used as an alternative method for precision, comparison and verification. In this case, the signal analysis software provided with this device can be used to demodulate and acquire the input and output signals separately. The signals can then be synchronized by correlating them with the original signal of Matlab.

4.2.2 Experimental results

Measurements have been carried out on a PA from the market, the ZFL 2500 from Mini-circuits. This wide-band (500-2500 MHz) PA is used in several types of applications, typically in GPS and cellular base stations. According to its data sheet, it has a typical output power of 15 dBm at 1 dB gain compression, and a small signal gain of 28 dB (± 1.5). The modulation adopted through the measurements is 16 QAM. The pulse shaping filters are raised cosine filters with a roll-off factor of 0.35 extending 4 symbols on either side of the center tap and 20 times oversampled. The carrier frequency is 1.8 GHz and the bandwidth 4 MHz. In order to acquire a sufficient number of samples for an accurate PD identification, 5 sequences of 100 symbols (2k samples) each, have been generated and sent to the VSG successively, i.e. a total number of 10k samples have been used for identification and evaluation.

Static power measurements

In order to validate the study presented in Sec. 3, we have performed the one- and two-tone tests on this PA. The defined parameters, namely, compression and interception points and the output saturation power, are also very useful for the experimental evaluation of the DPD technique. Figure 14 shows the AM/AM characteristic of the PA under test, its compression points and the corresponding power series model identified using the development presented in sec-

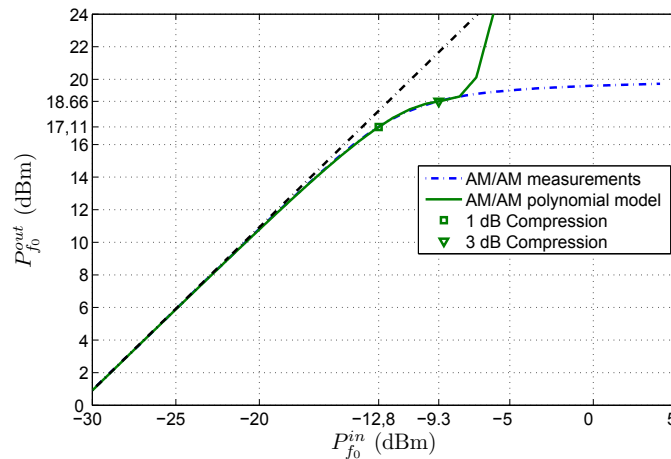


Fig. 14. RF polynomial model of the ZFL-2500 PA extracted from static power measurements (compression and interception points)

P_{1dB}^{out}	17.11 dBm
P_{3dB}^{out}	18.66 dBm
P_{sat}^{out}	19.73 dBm
IP_3^{out}	29.46 dBm

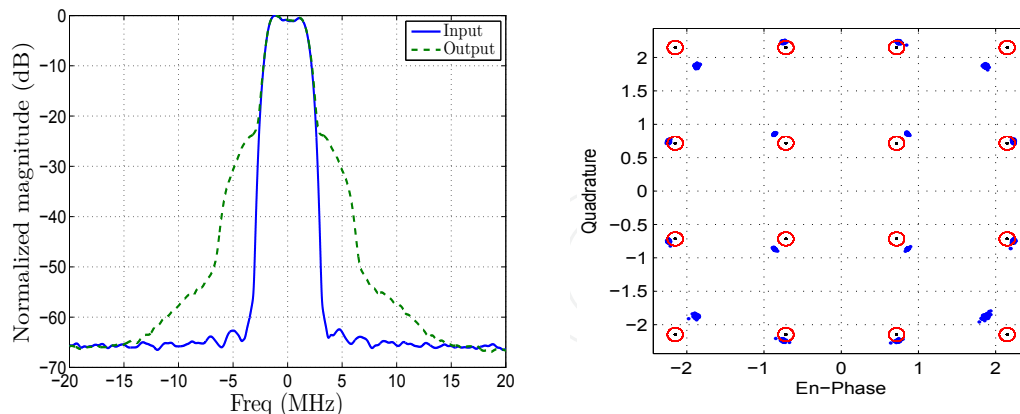
Table 1. Parameters from the static power measurements

tion 3. As we can see from this figure, the power series model fits well the measured AM/AM characteristic up to approximately the 4 dB compression point, after which it diverges. Table 1 shows the different parameters measured from the one- and two-tone tests at the carrier frequency of 1.8 GHz.

Nonlinearity on modulated signals

In the first part of this chapter, we have analyzed amplitude nonlinear distortion of PAs on special excitation signals, the one- and two-tone signals. We have observed that, in the case of a two-tone excitation, some frequency components, the intermodulation products (IMPs), appear very close to the fundamental frequencies and consequently cannot be rejected by filtering. If the number of tones increases in the excitation signal, approaching thus real communications bandpass signals (Sec. 3.3), the number of IMPs increases drastically. Here, a simple quantification of the nonlinearity at one IMP becomes no more sufficient to appropriately represent the real distortion incurred on such a signal. In fact, the IMPs fall inside or very close to, the bandwidth of the original signal, causing in band and out of band distortions.

Fig. 15 shows the input/output spectra of the ZFL-2500 PA, and the constellation of its output signal for an average output power equal to 16.52 dBm. As shown in Fig. 15a, the out of band distortion appears as spurious components in the frequency domain in the vicinity of the original signal bandwidth, which is often referred by *spectral regrowth*. In real communications, this out of band distortion may result in unacceptable levels of interference to other users, which is often quantified by the ACPR parameter. On the other hand, the in band distortion appears on the warped constellation of the output signal, as shown in Fig. 15b, where the constellation points are no more located on a rectangular grid. This may increase the bit error rate (BER) in the system, and is measured by the EVM parameter.



(a) Input and output spectra of the ZFL-2500 PA, (b) Constellation at the output of the ZFL-2500 PA, EVM $\approx 10.32\%$
ACPR ≈ -30 dB

Fig. 15. Nonlinear distortion on modulated signals, $P_{avg}^{out} \approx 16.52$ dBm

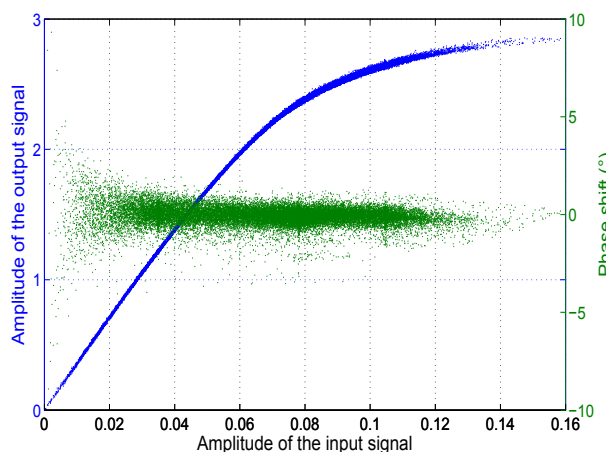


Fig. 16. Dynamic AM/AM et AM/PM characteristics of the ZFL-2500 PA

Rapp model

The dynamic AM/AM and AM/PM characteristics of the ZFL-2500 PA are shown in Fig. 16. They are defined as being, respectively, the instantaneous amplitude variation of the output signal $|\tilde{y}(n)|$, and the instantaneous phase shift $\varphi(n) = \angle\tilde{y}(n) - \angle\tilde{x}_i(n)$, in function of the instantaneous amplitude of the input signal $|\tilde{x}_i(n)|$. Although a relatively high dispersion appears on the AM/PM characteristic, the nonlinear phase distortion can be considered as negligible on the whole input amplitude range. It is a typical characteristic of low power Solid State PAs (SSPAs), which generally do not present strong memory effects. The quasi-memoryless Rapp model (Rapp, 1991) is often used in this case to model such PAs. Assuming that the phase distortion is negligible, the output signal may be expressed as follows

$$\tilde{y}(n) = G(|\tilde{x}_i(n)|)\tilde{x}_i(n) \quad (52)$$

where

$$G(|\tilde{x}_i(n)|) = \frac{K_r}{\left(1 + \left(\frac{K|\tilde{x}_i(n)|}{A_{sat}}\right)^{2p}\right)^{1/2p}} \quad (53)$$

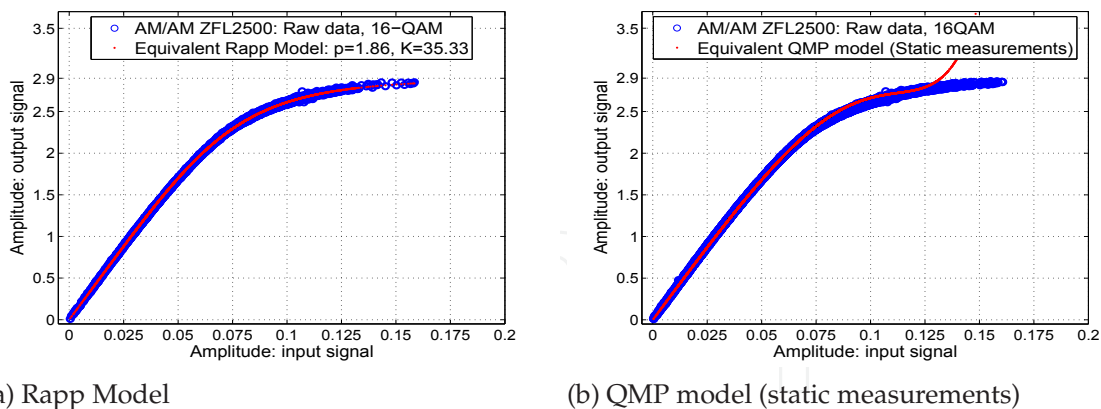


Fig. 17. ZFL-2500 models: Rapp identified from the acquired samples of the 16-QAM modulated signal, and the QMP model extracted from the measured compression and interception points (Sec. 3)

is the gain function of the PA, K_r the small signal gain, A_{sat} the saturation amplitude at the output, and $p > 0$ a parameter to control the transition form of the AM-AM curve between the linear region and saturation. The Rapp model corresponding to the ZFL-2500 PA has been identified from the acquired input/output samples, with a 16QAM excitation signal. In Fig. 17 we show the dynamic AM-AM characteristics of the ZFL-2500 and its corresponding Rapp model (Fig. 17a). For comparison, we present also on Fig. 17b the AM-AM characteristic of the quasi-memoryless polynomial (QMP) model. The latter is identified from the static measurements (one- and two-tone tests) and relying on the theoretical development presented in the first part of this chapter. One could obviously notice that the Rapp model fits better the measured dynamic AM/AM characteristic than the QMP model. However, we should not forget that the QMP model is identified from a completely different excitation signals. When the signals acquisition, i.e. input/output samples, are not available, the QMP model could be useful for a first description of the behavior of the PA. Unlike the polynomial model, the Rapp model has the desirable property of being able to model the PA behavior close to saturation, that is, strong nonlinearities. While evaluating the DPD technique we are particularly interested in its linearity performance near saturation where the PA reaches its highest power efficiency. For this reason we will adopt the Rapp model, as mentioned before, for a first evaluation via simulations.

Predistorter Performance

For simplicity, the characteristic function of the PD, $F(\cdot)$, has been implemented using a constant gain Look-Up-Table (LUT) (Cavers, 1990) in simulations and measurements. Figure 18 shows the ACPR performance over a varying output power values in simulations (Fig. 18a) and in measurements (Fig. 18b). In both cases, the maximum correction is achieved at an output power close to 12 dBm. Simulations were conducted with a very high precision, using 80k samples and a sweep power step equal to 0.1 dB. We can conclude first that measurements and simulations results are of high agreement. While a correction of 19 dB could be achieved in simulations, a close improvement has been reached in measurements of 17.5 dB. The small disagreement between simulations and measurements is due to unavoidable noise effects.

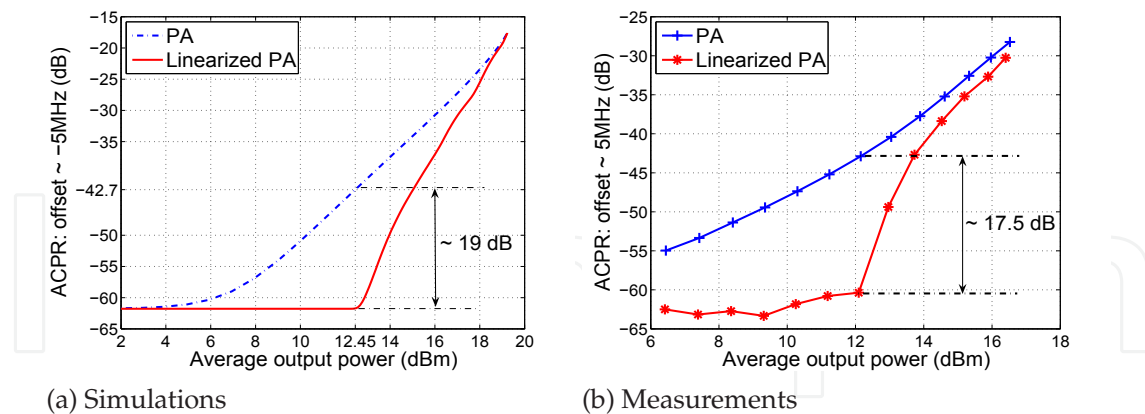


Fig. 18. ACPR performance vs output power of the PA without and with linearization

We can notice from figure 18 the rapid deterioration in the performance of the PD for an output power greater than 12.45 dBm. In fact, from the knowledge of the output saturation power of the PA, we can determine the maximum theoretical output power of the linearized power amplifier (LPA), denoted P_{max}^{lin} . This power corresponds to the minimum backoff value, OBO_{min}^{lin} for an ideal amplification of the cascade PD and PA. In fact, knowing the saturation power at the output of the PA P_{sat}^{out} and the PAPR of the input signal, it is easy to show that $P_{max}^{lin} = P_{sat}^{out} - PAPR$. In our case, the PAPR of the 16QAM modulated signal, filtered by a raised cosine pulse shaping filter, is equal to 7.25 dB (20 times averaging, 500 ksymbols). The output saturation power has been found equal to 19.7 dBm (Tab. 1). Thus, $P_{max}^{lin} = 12.45$ dBm and $OBO_{min}^{lin} = PAPR = 7.25$ dB. If the output power exceeds P_{max}^{lin} , the signal will reach the saturation of the PA, which is a very strong nonlinearity and will deteriorate rapidly the performance of the PD. We can deduce that by reducing the PAPR of the input signal, i.e. its envelope variation, smaller values of backoff could be used, and hence, approaching the maximum power efficiency of the PA. Most of the linearization systems today, combine special techniques to reduce the PAPR of the modulated signals to linearization techniques. Finally, from the above results, we can say that the DPD technique could have linearization performances very close to ideal, if the system is provided with sufficiently digital power processing.

5. Conclusion

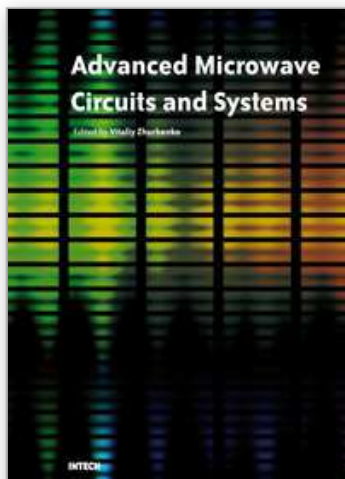
PA nonlinearity is a major concern in the realization of modern communications systems. In this chapter, we have provided some of the basic knowledge on power amplifier nonlinearity and digital baseband predistortion technique. In the first part the traditional power series analysis was repeated with a new interesting development in frequency domain. This analysis was validated in simulations under Matlab and through measurements on a real PA. The second part of this chapter was dedicated to a brief overview on the adaptive digital baseband predistortion technique and an experimental evaluation of this technique. A fully automatic test bench was used.

The most interesting perspective of this study is make further generalization of the power analysis when more complicated signals are used. For the digital predistortion techniques,

there remain a lot of efforts to deploy, especially on fast adaptation algorithms, and nonlinear memory effects modeling accuracy.

6. References

- Benedetto, S. & Biglieri, E. (1999). *Principles of Digital Transmission: With Wireless Applications*, Kluwer Academic Publishers, Norwell, MA, USA.
- Black, H. (1928). Translating system, US Patent, number 1,686,792.
- Black, H. (1937). Wave translation system, US Patent, number 2,102,671.
- Bosch, W. & Gatti, G. (1989). Measurement and simulation of memory effects in predistortion linearizers, *Microwave Theory and Techniques, IEEE Transactions on* **37**(12): 1885–1890.
- Cavers, J. (1990). Amplifier linearization using a digital predistorter with fast adaptation and low memory requirements, *Vehicular Technology, IEEE Transactions on* **39**(4): 374–382.
- Cripps, S. C. (2006). *RF Power Amplifiers for Wireless Communications, Second Edition (Artech House Microwave Library (Hardcover))*, Artech House, Inc., Norwood, MA, USA.
- Haykin, S. (2005). Cognitive radio: brain-empowered wireless communications, *Selected Areas in Communications, IEEE Journal on* **23**(2): 201–220.
- Ibnkahla, M. (2000). Neural network predistortion technique for digital satellite communications, *Acoustics, Speech, and Signal Processing, 2000. ICASSP '00. Proceedings. 2000 IEEE International Conference on* **6**: 3506–3509 vol.6.
- Isaksson, M., Wisell, D. & Ronnow, D. (2005). Wide-band dynamic modeling of power amplifiers using radial-basis function neural networks, *Microwave Theory and Techniques, IEEE Transactions on* **53**(11): 3422–3428.
- Isaksson, M., Wisell, D. & Ronnow, D. (2006). A comparative analysis of behavioral models for rf power amplifiers, *Microwave Theory and Techniques, IEEE Transactions on* **54**(1): 348–359.
- Kenington, P. (2002). Linearized transmitters: an enabling technology for software defined radio, *Communications Magazine, IEEE* **40**(2): 156–162.
- Kenington, P. B. (2000). *High Linearity RF Amplifier Design*, Artech House, Inc., Norwood, MA, USA.
- Liu, T., Boumaiza, S. & Ghannouchi, F. (2004). Dynamic behavioral modeling of 3g power amplifiers using real-valued time-delay neural networks, *Microwave Theory and Techniques, IEEE Transactions on* **52**(3): 1025–1033.
- Mitola, J. (1995). The software radio architecture, *Communications Magazine, IEEE* **33**(5): 26–38.
- Morgan, D., Ma, Z., Kim, J., Zierdt, M. & Pastalan, J. (2006). A generalized memory polynomial model for digital predistortion of rf power amplifiers, *Signal Processing, IEEE Transactions on* **54**(10): 3852–3860.
- Rapp, C. (1991). Effects of HPA-nonlinearity on a 4-dpsk/ofdm-signal for a digital sound broadcasting system, *Proc. 2nd Eur. Conf. Satellite Communications, Liege, Belgium* pp. 179–184.
- Schetzen, M. (2006). *The Volterra and Wiener Theories of Nonlinear Systems*, Krieger Publishing Co., Inc., Melbourne, FL, USA.
- Wood, J., Root, D. & Tufillaro, N. (2004). A behavioral modeling approach to nonlinear model-order reduction for rf/microwave ics and systems, *Microwave Theory and Techniques, IEEE Transactions on* **52**(9): 2274–2284.



Advanced Microwave Circuits and Systems

Edited by Vitaliy Zhurbenko

ISBN 978-953-307-087-2

Hard cover, 490 pages

Publisher InTech

Published online 01, April, 2010

Published in print edition April, 2010

This book is based on recent research work conducted by the authors dealing with the design and development of active and passive microwave components, integrated circuits and systems. It is divided into seven parts. In the first part comprising the first two chapters, alternative concepts and equations for multiport network analysis and characterization are provided. A thru-only de-embedding technique for accurate on-wafer characterization is introduced. The second part of the book corresponds to the analysis and design of ultra-wideband low-noise amplifiers (LNA).

How to reference

In order to correctly reference this scholarly work, feel free to copy and paste the following:

Mazen Abi Hussein, Yide Wang and Bruno Feuvrie (2010). Distortion in RF Power Amplifiers and Adaptive Digital Base-Band Predistortion, *Advanced Microwave Circuits and Systems*, Vitaliy Zhurbenko (Ed.), ISBN: 978-953-307-087-2, InTech, Available from: <http://www.intechopen.com/books/advanced-microwave-circuits-and-systems/distortion-in-rf-power-amplifiers-and-adaptive-digital-base-band-predistortion>

INTECH

open science | open minds

InTech Europe

University Campus STeP Ri
Slavka Krautzeka 83/A
51000 Rijeka, Croatia
Phone: +385 (51) 770 447
Fax: +385 (51) 686 166
www.intechopen.com

InTech China

Unit 405, Office Block, Hotel Equatorial Shanghai
No.65, Yan An Road (West), Shanghai, 200040, China
中国上海市延安西路65号上海国际贵都大饭店办公楼405单元
Phone: +86-21-62489820
Fax: +86-21-62489821

© 2010 The Author(s). Licensee IntechOpen. This chapter is distributed under the terms of the [Creative Commons Attribution-NonCommercial-ShareAlike-3.0 License](#), which permits use, distribution and reproduction for non-commercial purposes, provided the original is properly cited and derivative works building on this content are distributed under the same license.

IntechOpen

IntechOpen